Publications

7-25-2014

Nonadiabatic Heating in Magnetic Reconnection

Xuanye Ma
University of Alaska, Fairbanks, max@erau.edu

Antonius Otto
University of Alaska, Fairbanks

Journal of Geophysical Research: Space Physics

Nonadiabatic heating in magnetic reconnection

Xuanye Ma[1] and Antonius Otto[1]

[1]Geophysical Institute, University of Alaska Fairbanks, Fairbanks, Alaska, USA

Abstract Plasma transport process as a fundamental problem in magnetospheric physics is often associated with strong nonadiabatic heating. At the magnetopause, observations show an increase of specific entropy (i.e., $S = p/\rho^\gamma$) by 2 orders of magnitude from the magnetosheath into the magnetosphere. In the near-Earth magnetotail, particle injection requires strongly entropy depleted plasma bubbles, and their evolution can be strongly modified in the presence of nonadiabatic heating. In this study, one of the critical plasma transport mechanisms, magnetic reconnection, is investigated as a nonadiabatic process in the framework of MHD. It is important to examine whether magnetic reconnection can provide sufficient nonadiabatic heating to explain the observed plasma properties and to identify plasma conditions that allow such strong nonadiabatic heating. We demonstrate that the entropy can indeed strongly increase associated with magnetic reconnection provided that the plasma beta (i.e., the ratio of thermal to magnetic energy density) is low in the inflow region of reconnection.

1. Introduction

Magnetic reconnection is a fundamentally important process in space physics, because it converts the stored magnetic energy into the kinetic energy and changes the magnetic topology such that plasma can be transported across magnetic boundaries [*Dungey*, 1961; *Parker*, 1957; *Sweet*, 1958]. It occurs in the presence of sufficiently large antiparallel magnetic field components. At the dayside magnetopause, magnetic reconnection is the prime mechanism for a transfer of magnetic flux and energy into the magnetosphere during periods of southward interplanetary magnetic field (IMF). During times of northward IMF, magnetic reconnection occurs at higher latitudes [*Kessel et al.*, 1996]. The concept of magnetic reconnection is based on the breakdown of the so-called "frozen-in" condition. In Petschek's reconnection model [*Petschek*, 1964], the frozen-in condition breaks in a tiny diffusion region, which is bound by inflow and outflow regions. The inflow and outflow regions are separated by two pairs of slow shocks (see Figure 1), where the plasma is mostly accelerated by the $\mathbf{j} \times \mathbf{B}$ force and magnetic energy is converted into bulk and thermal energy.

The energy conversion is one of the most important aspects of magnetic reconnection. This process can also be considered as a nonadiabatic process, which can be characterized by a variety of computable plasma entropy measures [*Balasis et al.*, 2009; *Kaufmann and Paterson*, 2009]. In this study, we focus on the so-called "specific entropy," $S = p/\rho^\gamma$, where p is the plasma thermal pressure, ρ is the plasma density, and $\gamma = 5/3$ is the ratio of specific heats [*Birn et al.*, 2006, 2009]. Hereafter, we simply refer to this quantity as entropy. Note that a value of $\gamma = 5/3$ corresponds to 3 degrees of freedom for the motion of charged particles. In the MHD description, entropy is an invariant in the absence of Ohmic or viscous heating and shocks. Nevertheless, in the context of magnetic reconnection, the breakdown of ideal MHD by local dissipation also implies a breakdown of the entropy conservation. A significant entropy increase in Petschek's model may be provided by the two pairs of slow shocks bounding the outflow regions. These represent the major entropy sources, as will be demonstrated in this study for different types of reconnection geometries.

It is believed that magnetic reconnection is the dominant process for southward IMF conditions. For northward IMF conditions, reconnection driven by nonlinear Kelvin-Helmholtz modes at the low-latitude boundary layer and high-latitude reconnection become more important [*Scholer and Treumann*, 1997]. On the other side, satellite observations show that ions in the Earth's plasma sheet become cold and dense during prolonged periods of northward IMF, which has been attributed to the massive transport of the solar wind or magnetosheath ions into the plasma sheet [*Fujimoto et al.*, 1997]. There are two components of plasma in this cold dense plasma sheet, a hot distribution, which is considered a remnant of the original plasma sheet plasma, and a cold distribution, which is believed to be of magnetosheath origin [*Wang et al.*, 2007]. The typical flank magnetosheath ion density and temperature for fast solar wind conditions
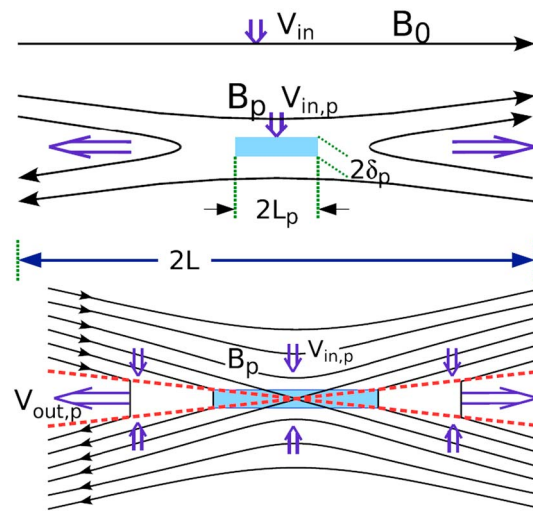
Figure 1. Illustration of the Petschek reconnection geometry. (top) Length scales assumed in Petschek's model and (bottom) illustration of the diffusion region and the attached slow shocks [*Otto*, 2012].

are about 5 cm^{-3} and 50 eV. For slow solar wind conditions, the ion density and temperature are about 8 cm^{-3} and 10 eV [*Borovsky and Cayton*, 2011]. Density and temperature for the cold plasma component are about 0.5 cm^{-3} and 500 eV [*Wang et al.*, 2007], which yield an entropy increase of about 1 to 2 orders of magnitude compared to the magnetosheath. Therefore, the plasma entry process is accompanied with strong nonadiabatic heating. One may expect that this nonadiabatic heating is mainly caused by magnetic reconnection, because reconnection is believed to be the prime mechanism for this entry process. However, studies by *Birn et al.* [2006, 2009] and *Wing and Johnson* [2009] demonstrated that entropy appears more or less unchanged after reconnection. This raises the important question, can magnetic reconnection provide any significant nonadiabatic heating? Directly related is the issue of any specific conditions, for which significant nonadiabatic heating may occur.

Here we present a systematic study of the entropy changes in magnetic reconnection based on analytical theory and numerical MHD simulation. The numerical methods are introduced in section 2. In section 3, we discuss entropy sources in different subregions in a Petschek-type reconnection geometry. For applications to the actual magnetospheric boundary, the influence of a guide field, of an asymmetry in the inflow regions, and of the shear flow are discussed in section 4. Section 5 presents a summary and discussion.

2. Numerical Model

The full set of the resistive MHD equations and its numerical solver have been discussed by *Otto* [1990]. In the computations all quantities are normalized to the typical values, that is, the length scales L to a typical length L_0, the density ρ to $\rho_0 = n_0 m_0$ with the number density n_0 and the ion mass m_0, the magnetic field **B** to B_0, the velocity **V** to the typical Alfvén velocity $V_A = B_0/\sqrt{\mu_0 \rho_0}$, the thermal pressure p to $P_0 = B_0^2/(2\mu_0)$, and the time t to a typical Alfvén transit time $T_A = L_0/V_A$. To enclose MHD equations, one can use either the entropy equation (1)

$$\frac{\partial h}{\partial t} = -\nabla \cdot (h\mathbf{V}) + \frac{\gamma - 1}{\gamma} h^{1-\gamma} \eta j^2, \tag{1}$$

where $h = (p/2)^{1/\gamma}$ or the energy equation (2):

$$\frac{\partial w}{\partial t} = -\nabla \cdot \left[\left(w + \frac{1}{2} p_t \right) \mathbf{V} - (\mathbf{V} \cdot \mathbf{B}) \mathbf{B} + \eta \mathbf{j} \times \mathbf{B} \right], \tag{2}$$

where $w = \left[\rho v^2 + B^2 + p/(\gamma - 1) \right]/2$ is the total energy density of the plasma, and $p_t = (p + B^2)$ is the total pressure. Note that in this normalization, the unitless entropy is $S = p/(2\rho^\gamma)$. The difference between the energy equation and the entropy equation will be discussed in section 3.1.1.

We present the results from four selected two-dimensional simulations to study the entropy enhancement for typical magnetic reconnection configurations using a symmetric reference case and including characteristic variations in terms of the magnetic field, plasma flow, and symmetry of the configuration. The simulation domain is a rectangular box with $|x| \leq 20$, and $0 \leq y \leq 80$, and is resolved by using 323×353 grid points with a nonuniform grid in both directions. To sufficiently resolve the diffusion region, the best resolution is set to 0.025 and 0.1 in the x and y direction in the diffusion region. Free boundary conditions ($\partial_n = 0$, where ∂_n is the partial derivative in the direction normal to the boundary) are applied to the x maximum and minimum boundary and y maximum boundary. The y minimum boundary is determined by symmetry properties of the MHD equations [*Otto et al.*, 2007]. The initial equilibrium is a one-dimensional

Table 1. Values of the Simulation Parameters

Case	ρ_0	$\delta\rho$	B_g	V_{zi}	p_∞
A	1	0	0	0	0.1
B	1.5	0.5	0	0	0.025
C	1	0	1	0	0.1
D	1	0	0	0.5	0.1

modified Harries sheet [*Harris*, 1962], which is given by $\mathbf{B} = \tanh(x)\hat{\mathbf{e}}_y + B_g\hat{\mathbf{e}}_z$, $\mathbf{V} = V_{zi}\tanh(x)\hat{\mathbf{e}}_z$, $p = p_\infty + 1 - B_y^2$, $\rho = \rho_0 + \delta\rho\tanh(x)$, where the parameters B_g, V_{zi}, and $\delta\rho$ are used to introduce a guide field, flow shear, and density asymmetry. The values of all parameters are listed in Table 1. To trigger Petschek-type magnetic reconnection (except case B), we use a localized resistivity given by

$$\eta = \eta_0 \left[1 - \exp\left(-t/\tau\right)\right] \cosh^{-1}(x) \cosh^{-1}(y) + \eta_b, \qquad (3)$$

where $\eta_0 = 0.05$, $\tau = 5$, and the small background resistivity $\eta_b = 0.002$.

Case A is the reference case. At the real magnetopause, the magnetosheath density is about 10 times larger than the magnetospheric density. Therefore, it is important to investigate this asymmetry for the entropy production. In the simulation (case B), we set $p_\infty = 0.025$, $\rho_0 = 1.5$, and $\delta\rho = 0.5$, which yields to ρ_{MSP} : $\rho_{MSH} = 1 : 2$, where ρ_{MSP} refers to the magnetosphere ($x < 0$) density, and ρ_{MSH} is the magnetosheath ($x > 0$) density. We only localized the resistivity along the y direction, because the diffusion region may move along the x direction:

$$\eta = \eta_0 \left[1 - \exp\left(-t/\tau\right)\right] \cosh^{-1}(y) + \eta_b. \qquad (4)$$

At dayside magnetopause, a guide field or a large perpendicular shear flow is always present. The influence of a guide field and of shear flow on the entropy production is investigated in the cases C and D, respectively.

3. Symmetric Petschek Reconnection

Figure 2 shows the thermal pressure (left) at $t = 150$ for Case A. In the inflow region, the pressure is about 0.1 (the reddish region in Figure 2), which yields an initial inflow region plasma beta of 0.1. In the outflow region, the pressure increases to about unity (the greenish region in Figure 2). Black lines are magnetic field lines (contours for the z component of the vector potential). The strongly bend magnetic field lines at the transition between inflow and outflow regions illustrates the presence of a strong surface current, and the inspection of the plasma properties (section 3.1) of the inflow and outflow regions demonstrates that this boundary represents a slow switch-off shock. Black arrows represent the flow velocity. The inflow velocity only has a normal component (x direction) with a relatively small magnitude, and it carries flux into the outflow region. The fast jetting plasma in the outflow region reaches the inflow Alfvén speed, which indicates that reconnection is well developed. There are three subregions [*La Belle-Hamer et al.*, 1995] that can be identified in the outflow region. The diffusion region is located at the origin ($x = y = 0$), and it is barely visible in Figure 2, which is consistent with the assumption of a small diffusion region in Petschek's model [*Petschek*, 1964]. The steady outflow region ($y < 50$ in Figure 2) is bounded by a pair of slow shocks being characterized by the thin current layers. And the nonsteady bulge region ($y > 50$ in Figure 2) is the transition region between the fast reconnection jet and the unperturbed plasma.

3.1. The Dominant Entropy Source: Slow Shocks at the Steady Outflow Region

The transition between the inflow and outflow regions is almost one-dimensional, because the angle of the shocks with the y axis is small, and the transition represents the matching of the two asymptotic plasma conditions of the inflow regions by MHD waves and discontinuities (the so-called "Riemann problem" [*Lin and Lee*, 1993]). In Figure 2 (right), we present a profile of this transition layer ($x \geq 0$ part of the cut, due to the symmetry), where the cut is taken from the blue line in Figure 2 (left). The five panels in Figure 2 (right) show the profiles of the plasma density, thermal pressure, normalized entropy, S/S_0, the magnetic field B_y component, and current density z component. Here $S_0 = 0.05$ is the inflow region entropy. The depletion of the density in the vicinity of the y axis, (shaded in gray and labeled as D in Figure 2) is a contact discontinuity and its cause will be discussed in section 3.2. The large current density is consistent with the switch off of the magnetic field, which indicates that these current layers represent the slow switch-off shock layers. These shock layers are shaded in gray and labeled S in Figure 2. A slow shock in the reconnection layer of the dayside magnetopause has for instance been observed by ISEE 2 spacecraft [*Walthour et al.*, 1995].
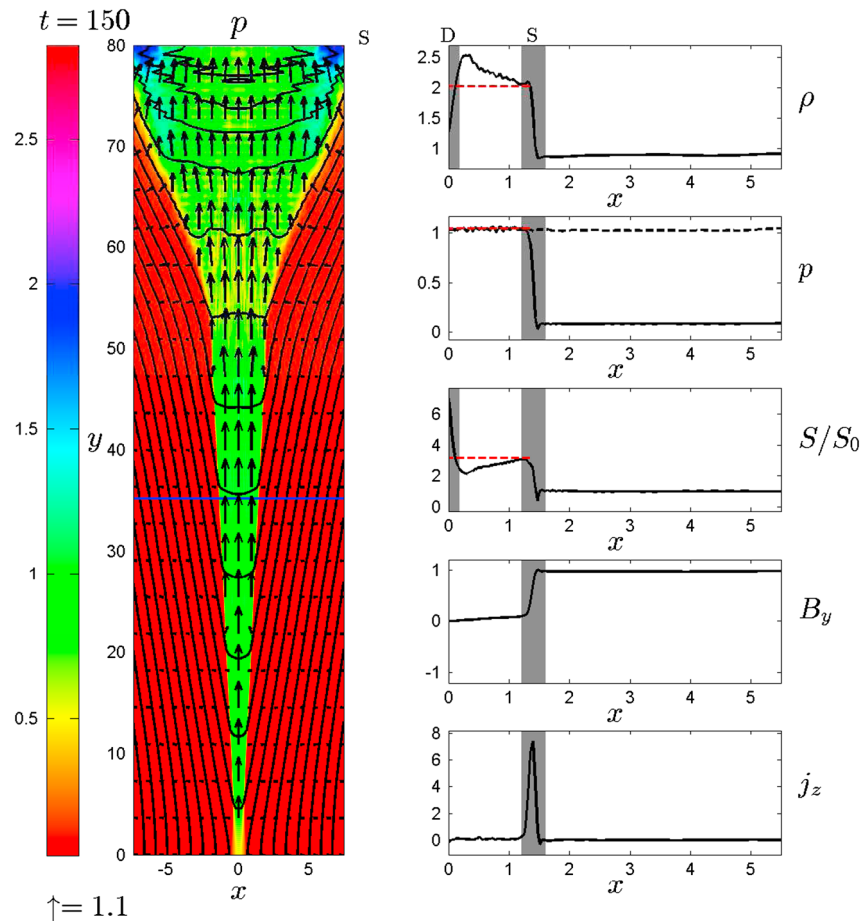
Figure 2. (left) The thermal pressure p at $t = 150$ for Case A. Black lines are the magnetic field lines (contours for the z component of the vector potential), and black arrows indicate the flow velocity **V**. (right) The five panels show the profiles of the plasma density, thermal pressure, normalized entropy, S/S_0, magnetic field B_y component, and current density j_z component, which are taken from the blue line in Figure 2 (left). The red dashed lines are the results from the Rankine-Hugoniot (RH) relations. The black dashed line is the total pressure. The slow shock and density depletion layer are shaded in gray and labeled S and D, respectively.

The plasma density, thermal pressure, and entropy strongly increase through the shock layers, while the total pressure (black dashed line in the pressure plot) remains constant across the shock layers. The properties of the slow switch-off shock can be described by the so-called "Rankine-Hugoniot (RH) relations," which are inferred from MHD equations (enclosed by energy equation) with homogeneous assumption for both upstream and downstream. Here we list the compression ratio, the ratio of downstream and upstream pressure and the corresponding ratio of the entropy for slow switch-off shocks:

$$\frac{\rho_d}{\rho_u} = 1 + \frac{1}{\gamma\beta + \gamma - 1}, \tag{5}$$

$$\frac{p_d}{p_u} = \frac{\rho_d}{\rho_u}\left(1 + \frac{\gamma - 1}{\gamma\beta}\right), \tag{6}$$

$$\frac{S_d}{S_u} = \left(\frac{\rho_d}{\rho_u}\right)^{1-\gamma}\left(1 + \frac{\gamma - 1}{\gamma\beta}\right), \tag{7}$$

where the index d and u indicate the downstream and upstream, respectively, and $\beta = p_u/B_u^2$ is the upstream plasma beta. Figure 3 presents the compression ratio, the ratio of downstream and upstream pressure, and the corresponding ratio of the entropy as a function of upstream plasma beta by using dash-dotted, dashed, and solid lines, respectively. Note that all the ratios increase with decreasing upstream
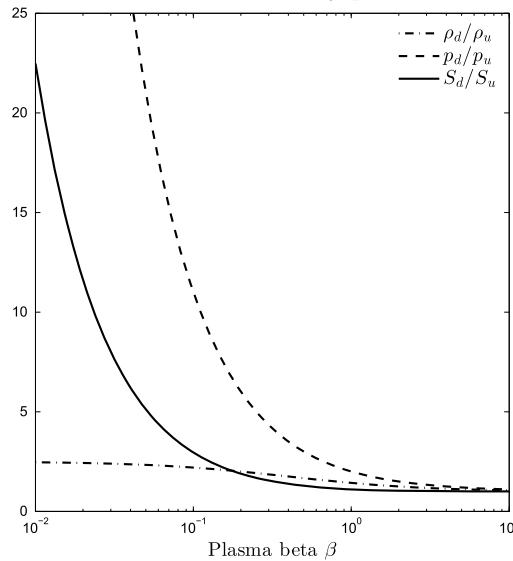
Figure 3. The ratio of downstream and upstream density (dash-dotted line), pressure (dashed line), and entropy (solid line) as a function of upstream plasma beta for the slow switch-off shock.

plasma beta, and the maximum plasma compression is 2.5, which means that the plasma entropy can increase significantly if the upstream plasma beta is sufficiently small. For $\beta < 10^{-2}$, the entropy ratio between outflow and inflow regions S_d/S_u is greater than 20.

To compare the theoretical results with the two-dimensional simulation results, we labeled the downstream results from the RH relations by the red lines in Figure 2. It shows that right after slow shock (downstream region), all quantities are consistent with the theoretical results, although density increases further deeper into the outflow region. This is possibly because fluid elements deep in the outflow region have entered much closer to the diffusion region at a location or time when the slow shock had not been fully developed. We carry out a one-dimensional simulation of the Riemann problem. This has the advantage of much higher resolution and short execution times. In this study, one-dimensional simulations are also used to compare the influence of different forms of the equation of state which closes the MHD equations.

3.1.1. Difference Between Energy Equation and Entropy Equation

The entropy equation (1) and the energy equation (2) are commonly used to model magnetic reconnection and other plasma problems. However, the RH conditions are based on the set of ideal MHD equations using energy conservation. Therefore, it is important to understand the implications of using the entropy equation (1) in resistive MHD particularly for applications involving nonadiabatic heating in magnetic reconnection.

The slow shock transition can be simulated in a one-dimensional configuration by adding a small constant B_n component in the Harries sheet [*Lin and Lee*, 1993, 1999; *Wu and Lee*, 2000; *Ma and Otto*, 2013]. The initial conditions are given by $\mathbf{B} = B_n\hat{\mathbf{e}}_x + \tanh(x)\hat{\mathbf{e}}_y$, $\mathbf{V} = 0$, $\rho = 1$, and initial plasma thermal pressure is determined by total pressure balance. Figure 4 presents the results from the one-dimensional simulation with the upstream plasma beta of 0.1. The three panels show the density (top), the thermal pressure (middle), and the entropy (bottom). The dashed and dash-dotted lines are the simulation results by using the entropy equation and energy equation, respectively. As a reference, the theoretical results from the RH relations (equations (5)–(7)) are labeled by the solid lines. For convenience, we have transformed the system to the shock frame. Thus, $x > 0$ is the upstream (inflow region) and $x < 0$ is the downstream (outflow region). Figure 4 shows that energy conservation yields correct jump relations; however, using the entropy equation generates an artificial density increase and an insufficient entropy change. Note that this density increase associated with the shock using entropy conservation satisfies mass conservation.

Clearly energy and entropy conservations generate different shock properties in ideal MHD ($\eta = 0$). The entropy increase through the shock is due to the energy conservation and does not require explicit Ohmic heating. However, the use of entropy conservation in ideal MHD strictly maintains entropy conservation and the resulting "slow shock equivalent" discontinuity is violating energy conservation. For resistive MHD ($\eta \neq 0$), the entropy equation (including the resistive term in equation (1)) allows entropy to increase through Ohmic heating. This can be shown clearly by combining the entropy equation and the continuity equation, which yields to

$$\frac{dS}{dt} = \frac{d}{dt}\left(\frac{p}{2\rho^\gamma}\right) = (\gamma - 1)\frac{\eta j^2}{\rho^\gamma}, \tag{8}$$

where $d/dt = \partial_t + \mathbf{V} \cdot \nabla$. Equation (8) indicates that a correct approximation to the slow shock solution is possible in the presence of sufficient Ohmic heating, which requires a very high resolution of the boundary
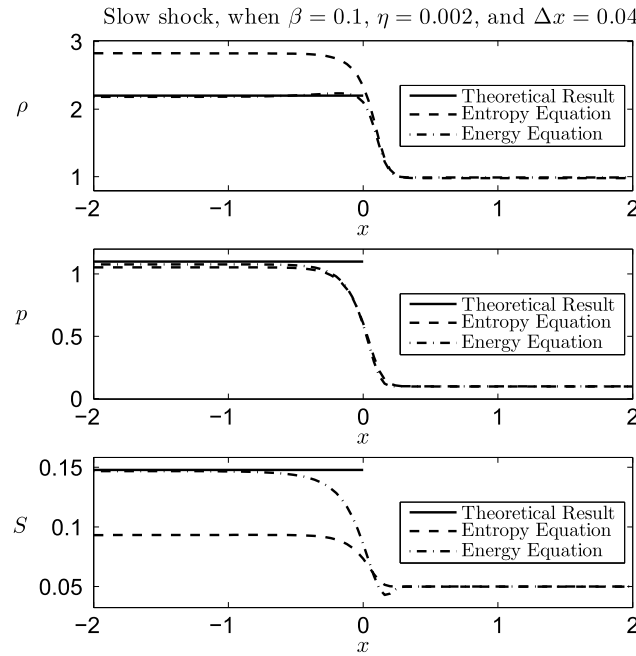
Figure 4. MHD slow shocks with upstream plasma beta of 0.1, and $\Delta x = 0.04$. The three panels show (top) the density, (middle) the thermal pressure, and (bottom) the entropy. The dashed and dash-dotted lines are the simulation results by using the entropy equation and energy equation, respectively. As the reference, the theoretical results from the RH relations are indicated by the solid lines.

between inflow and outflow regions in a numerical simulation. One can estimate the width of this resistivity layer δ by integrating both sides of equation (8)

$$\Delta S = (\gamma - 1)\frac{\eta j^2}{\rho^\gamma}\Delta t, \tag{9}$$

where $\Delta S = S_d - S_u \approx S_d = p_d \rho_d^{-\gamma}/2 = \rho_d^{-\gamma}/2, \rho = \rho_d, j \approx B/\delta = 1/\delta, \Delta t = \delta/v_n$, and $v_n = v_{An} \approx B_n/\sqrt{\rho_u} = B_n$, which yields

$$\delta \approx 2(\gamma - 1)\eta/B_n. \tag{10}$$

For the width of the shock current sheet if the dissipation is determined by a constant resistivity. This estimate uses normalized upstream values of $B = 1$, $\rho = 1$, and $p = \beta B^2 = 0.1$. In the cases of $\eta = 2\times10^{-3}$ and 1×10^{-3}, and $B_n = 0.025$, $\delta \approx 0.1$ and 0.05, respectively. The following results test equation (10) based on these parameters.

Figure 5 shows the compression ratio ρ_d/ρ_u (top) and entropy ratio S_d/S_u (bottom) as a function of the grid separation Δx in the one-dimensional slow

shock simulation by using the entropy equation. The solid lines indicate the theoretical results from the RH relations. A result from the energy equation by using resistivity $\eta = 2 \times 10^{-3}$ is labeled by stars. The circle and square markers are the results by using resistivity $\eta = 2 \times 10^{-3}$ and 1×10^{-3}, respectively. Figure 5 shows that the results from the entropy equation converge to the theoretical results for increasing resolution as indicated by our estimate for the required width of the current layer. However, a much higher resolution (20 times higher) has to be used for the simulation to achieve 90% of the correct entropy increase. The result demonstrates that the entropy equation with the resistive term can be used to model reconnection, but its use requires a large numerical effort to achieve an acceptable nonadiabatic heating. Therefore, the use of the energy equation appears much more appropriate for simulations involving shocks for all cases where the expected entropy increase is large.

3.1.2. Estimate of the Entropy Increase in the Magnetic Reconnection
It is demonstrated that slow switch-off shocks generate strong nonadiabatic heating for low upstream (inflow) plasma beta using analytical theory and simulation. However, this conclusion is based on one-dimensional shock configurations. To extend this argument to two-dimensional magnetic reconnection and more general inflow conditions including asymmetries requires a more general estimate. In magnetic reconnection, pressure balance implies

$$p_i + B_i^2 = p_o + B_o^2, \tag{11}$$

where i and o indicate the inflow and outflow region, respectively. Therefore, the entropy increase can be expressed as

$$\frac{S_o}{S_i} = \frac{p_o}{\rho_o^\gamma}\frac{\rho_i^\gamma}{p_i} = \left(\frac{p_i + B_i^2 - B_o^2}{p_i}\right)\left(\frac{\rho_i}{\rho_0}\right)^\gamma. \tag{12}$$

Since $B_o^2 \geq 0$, and $\rho_i < \rho_0$, due to compression, it follows that

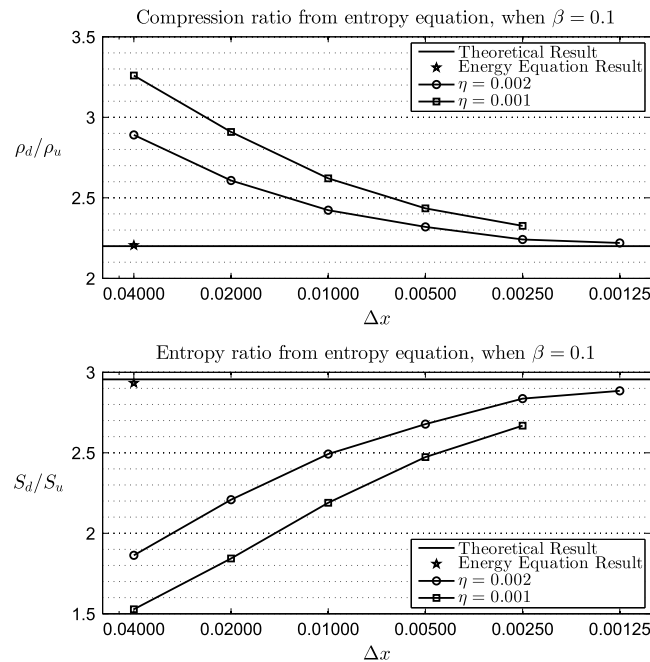$$S_o/S_i < 1 + 1/\beta_i, \tag{13}$$

Figure 5. The (top) compression ratio, ρ_d/ρ_u, and (bottom) entropy ratio, S_d/S_u, as a function of the grid separation, Δx, from the one-dimensional slow shock simulation by using the entropy equation. The solid lines indicate the theoretical results from the RH relations. A result for the energy equation by using resistivity $\eta = 2 \times 10^{-3}$ is labeled by a star. The circle and square markers are the results by using resistivity $\eta = 2 \times 10^{-3}$ and 1×10^{-3}, respectively.

where β_i is the inflow plasma beta. The physical interpretation is straightforward. The pressure balance determines that the thermal pressure in the outflow region and the thermal pressure ratio between outflow and inflow regions are large if the pressure is very small in the inflow region. Thus, large entropy increases are possible only for very small plasma beta in the inflow region.

In case A, the entropy increase is consistent with the RH relation (equation (7) gives $S_o/S_i = 2.95$). The estimate for entropy increase (equation (13)) gives an overestimate $S_o/S_i < 11$, because it does not take the compression into account. In the steady outflow region, the thermal pressure is almost identical with the total pressure (see the second panel in Figure 2 (right)), which is consistent with our assumption. Furthermore, we hypothesize that for the same inflow plasma beta β, this is the maximum possible entropy increase, i.e., the presence of shear flow or magnetic guide field cannot increase the entropy above this value.

3.2. Other Entropy Sources: The Diffusion Region and the Weak Fast Shock

The diffusion region is critical for the magnetic reconnection. In this region, the resistive term in Ohm's law is dominant, and nonadiabatic heating is prominent. Since the pressure is determined by total pressure balance with the inflow region, the density must decrease to balance the increasing plasma temperature. The low-density plasma is convected along stream lines. Due to the symmetry, the central streamline is the y axis, which is consistent with the result in Figure 2. This density depletion layer has also been reported in other reconnection simulations [*Ma and Bhattacharjee*, 2001; *Hesse et al.*, 2001; *Shay et al.*, 2001; *Pritchett*, 2001; *Yang et al.*, 2006]. However, the typical width of the diffusion region is on the order of an ion inertia scale for Hall physics and even smaller (electron inertia scale or gyroscale) in a kinetic model, which is negligible compared with macroscales of the whole system. Thus, we argue that the nonadiabatic heating in the diffusion region occupies a very small volume in a real space plasma and only a tiny fraction of the total plasma transported into the outflow region is actually going through the diffusion region. Therefore, only a small fraction of the plasma transported into the magnetosphere would be exposed to this nonadiabatic heating source.

The plasma in the steady outflow region is accelerated to the inflow region Alfvén speed by the slow switch-off shock. However, the plasma in the nonsteady bulge region moves at a velocity significantly lower than Alfvén speed. Due to the compression and heating, the acoustic speed in the outflow region can be lower than the velocity of the outflow jet. Therefore, it is possible for the fast shock to exist in the transition from the steady outflow to the bulge [*Zenitani and Miyoshi*, 2011] (in Figure 2, $y \in (50, 55)$). To characterize these fast shocks, we estimate the outflow region Mach number $M_o = V_o/c_{so}$, where V_o is outflow speed, which equates to the inflow Alfvén speed $V_{A_i} = B_i/\sqrt{\rho_i}$, and $c_{so} = \sqrt{\gamma p_o/(2\rho_o)}$ is the outflow acoustic speed. The pressure in the outflow region can be represented by the magnetic field in the inflow region from pressure balance $p_o = p_i + B_i^2$. By using the jump condition for density in a switch-off shock (equation (5)), we find

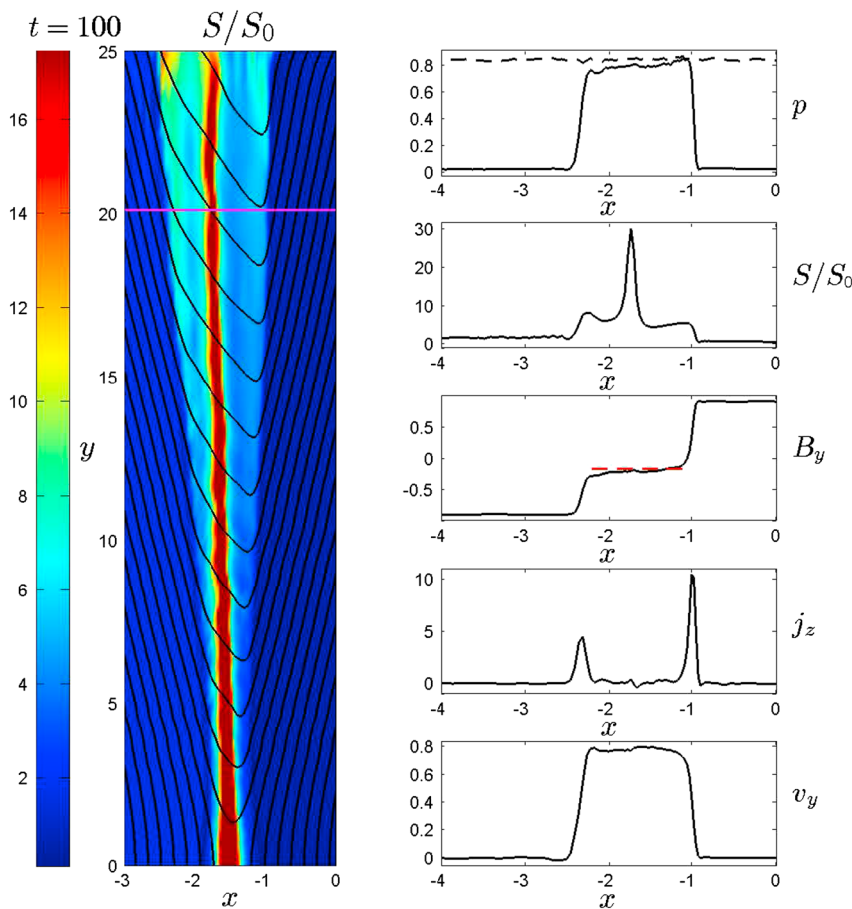$$M_o = \sqrt{2/(\gamma\beta_i + \gamma - 1)} \leq \sqrt{3}. \qquad (14)$$

Figure 6. (left) The normalized entropy at $t = 100$ for Case B. Black lines are the magnetic field lines. (right) The five panels show the profiles of the thermal pressure, normalized entropy, magnetic field B_y component, current density j_z component, and velocity V_y component, which are taken from the magenta line in Figure 6 (left). The total pressure is presented by a dashed line. The estimated value of B_o from equation (18) is indicated by a red dashed line.

This Mach number does not take into account the shock speed. Therefore, the actual Mach number is smaller, and a weak fast shock is not expected to be a significant source for the entropy increase. We note that in the high-resolution simulation by *Zenitani and Miyoshi* [2011], the maximum velocity of outflow jet in this fast shock region is higher than the inflow region Alfvén speed. However, the entropy remains almost constant across this fast shock.

4. More General Configurations

Although we have mostly discussed Petschek reconnection, the conclusions drawn from the estimate for the entropy increase (equation (13)) apply to more general and asymmetric configurations. In this section, we will discuss three different reconnection configurations, which more closely reflect to the real magnetopause geometry.

4.1. Asymmetric Density

An asymmetric configuration, with different densities and an inflow plasma beta of 0.025, is examined in case B. The normalized entropy S/S_0 at $t = 100$ is presented in Figure 6 (left), where S_0 is the initial magnetosheath side entropy ($x > 0$), which is $2^\gamma \approx 3.17$ times lower than magnetospheric entropy, due to the different densities. However, on both sides of the outflow region, entropy increases about 4 times compared to its original value. The magnetic field lines (the black contours in Figure 6 (left)) indicate that the slow shock on the magnetosheath side is replaced by an intermediate shock [*Yong and Lee*, 1990]. For a better illustration of the outflow, Figure 6 (right) shows profiles of the thermal pressure, normalized entropy, magnetic field B_y component, current density j_z component, and velocity V_y component, which are taken

from the magenta line in Figure 6 (left). The current density is higher on the magnetosheath side than on the magnetospheric side, which is consistent with the larger rotation of magnetic field on the magnetosheath side. This is caused by the larger inertia of the higher density magnetosheath material which requires a larger $\mathbf{j} \times \mathbf{B}$ force to change the momentum and accelerate the plasma into the outflow region [*La Belle-Hamer et al.*, 1995]. This also generates a nonzero outflow magnetic field $B_o = B_y \neq 0$, which contributes to the total pressure in the outflow region. The outflow total pressure (labeled by the dashed line in the first panel of Figure 6 (right)) is larger than the thermal pressure. Compared with the result from the RH relations, the entropy increase in the asymmetric case is less than the corresponding symmetric case.

The rigorous manner to determine B_y in the outflow region is to solve the Riemann problem [*Lin and Lee*, 1993, 1999]. However, a reasonable estimate of B_y in the outflow region can be obtained by assuming an approximately constant outflow velocity [*La Belle-Hamer et al.*, 1995], which is consistent with the fifth panel in Figure 6 (right). From the momentum equation and ignoring the pressure gradient along the y direction, we have

$$\rho \frac{dv_y}{dt} = j_z B_x. \tag{15}$$

By integrating both sides from the inflow region to outflow region

$$\Delta v_y = \int_{inflow}^{outflow} \frac{j_z B_x}{\rho} dt, \tag{16}$$

where $dt = dx/|v_x|$ and $v_x = V_{Ax} = B_x/\sqrt{\rho}$, which yields

$$\Delta v_y = \pm \int_{inflow}^{outflow} \frac{j_z}{\sqrt{\rho}} dx = \pm \frac{B_o - B_i}{\sqrt{\rho}}. \tag{17}$$

The "$\pm$" is determined by whether B_x is parallel or antiparallel to the shock normal direction. Here B_i and B_o are the tangential magnetic field components on the inflow and outflow sides at the outflow boundary. This equation ignores compressibility if the density is interpreted as the density in the respective inflow region. Alternatively, the density can be interpreted as suitable average density at the respective boundary, which, however, scales with the inflow density, inasmuch as the maximum compression is 2.5. We apply this equation to both sides of the boundary, which yields to

$$\frac{B_i - B_o}{\sqrt{\rho_1}} = \frac{B_o + B_i}{\sqrt{\rho_2}}$$

$$B_o = \frac{1-r}{1+r} B_i, \tag{18}$$

where ρ_1 and ρ_2 refers to the density of the two inflow regions (or a suitably averaged density if plasma compression is considered), and $r = \sqrt{\rho_1/\rho_2}$. Equation (18) shows that the magnitude of B_0 is always smaller than B_i, and B_o vanishes, if the density is symmetric ($\rho_1 = \rho_2$). Interchanging ρ_1 and ρ_2 changes the sign of B_o. The simulation result in Figure 6 uses a density ratio of $r = \sqrt{2}$ for the inflow regions, and B_o is indicated by red dashed line in the third panel in Figure 6 (right), which shows a good agreement with the simulation result. Combining equations (18) and (12), we obtain

$$\frac{S_o}{S_i} < 1 + \frac{1}{\beta} \frac{4r}{(1+r)^2}, \tag{19}$$

where S_i can be the entropy on either side. This relation (19) implies a reduction of the entropy increase in the presence of density asymmetry for the same inflow plasma beta.

4.2. Magnetic Shear

Magnetic reconnection without guide field is a singular situation in space plasma systems. A guide field component is present almost everywhere at the dayside magnetopause. In a two-dimensional configuration, the guide field component (B_z component in this study) does not change the reconnection dynamics significantly, because it can be considered as an additional pressure and is convected by the plasma. This B_z component often increases in the outflow region, which may cause the reduction of the entropy increase
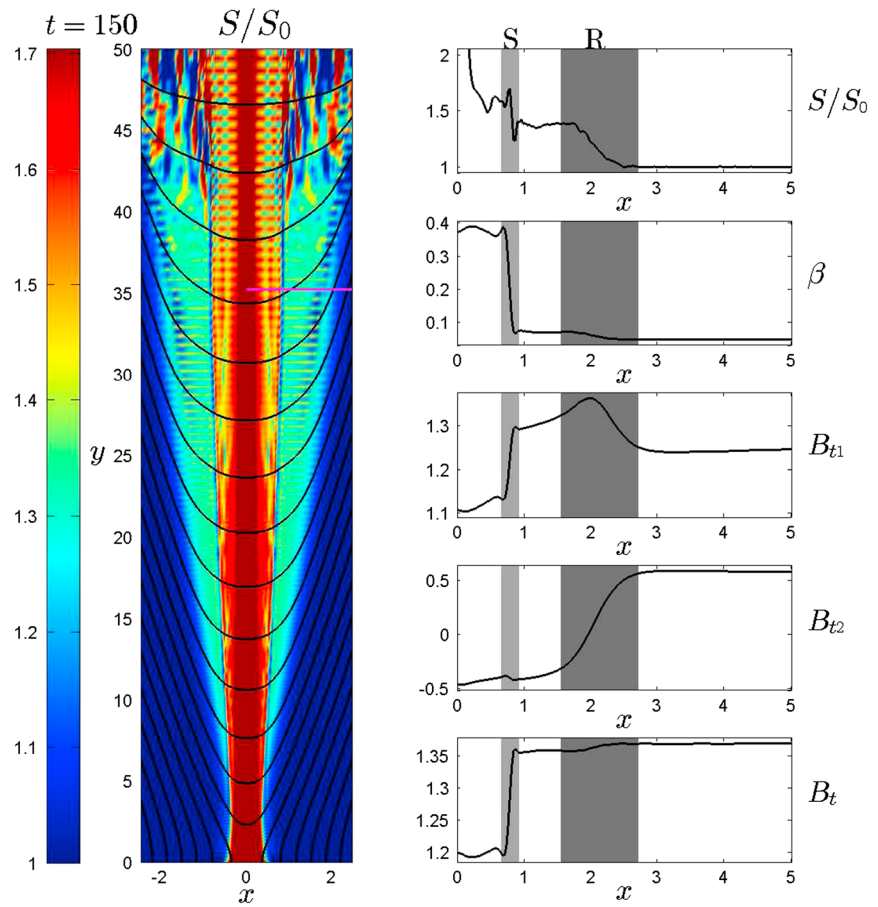
Figure 7. (left) The normalized entropy at $t = 150$ for Case C. Black lines are the magnetic field lines. (right) The five panels show the profiles of the normalized entropy, plasma beta, two components of the tangential magnetic field B_{t1} and B_{t2}, and the total tangential magnetic field, which are taken from the magenta line in Figure 7 (left).

in the outflow region. Figure 7 shows the results from Case C, where the initial configuration is the same as in Case A, except for the addition of a uniform guide field $B_z = 1$. Figure 7 (left) is the normalized entropy S/S_0 at $t = 150$, where S_0 is the inflow entropy. It shows that the outflow entropy is about 1.5 times higher than the inflow entropy, which is lower than in Case A. To better understand this transition region, a rigorous treatment is to solve the Riemann problem [*Lin and Lee*, 1993, 1999]. *Lin and Lee* [1993] demonstrated that the switch-off shock is replaced by a rotational discontinuity and a slow shock for a symmetric guide field, which is consistent with the observational results [*Biernat et al.*, 1998] and is also seen in our two-dimensional simulation. The five panels in Figure 7 (right) show the profiles of the normalized entropy, plasma beta, two components of the tangential magnetic field B_{t1} and B_{t2}, and the total tangential magnetic field $B_t = \sqrt{B_y^2 + B_z^2}$, which are taken from the magenta line in Figure 7 (left). Due to the symmetry, we only show the $x \geq 0$ part of the cut. For a better representation of the rotational discontinuity, we rotate the frame by an angle $\theta = \arctan\left(1/B_g\right)/2 = \pi/8$, thus

$$B_{t1} = B_z \cos\theta + B_y \sin\theta$$

$$B_{t2} = -B_z \sin\theta + B_y \cos\theta.$$

The rotational discontinuity layer is shaded in dark gray and labeled R, where B_{t1} is almost constant and B_{t2} changes from $+0.5$ to -0.5. Theoretically, the rotational discontinuity does not involve an entropy increase. However, the presence of the resistivity replaces the rotational discontinuity by an intermediate shock, thus leading to an increase in entropy and decrease in the total magnetic field, which is consistent with the results in Figure 7. The slow shock layer is shaded in light gray and labeled S, where the total tangential
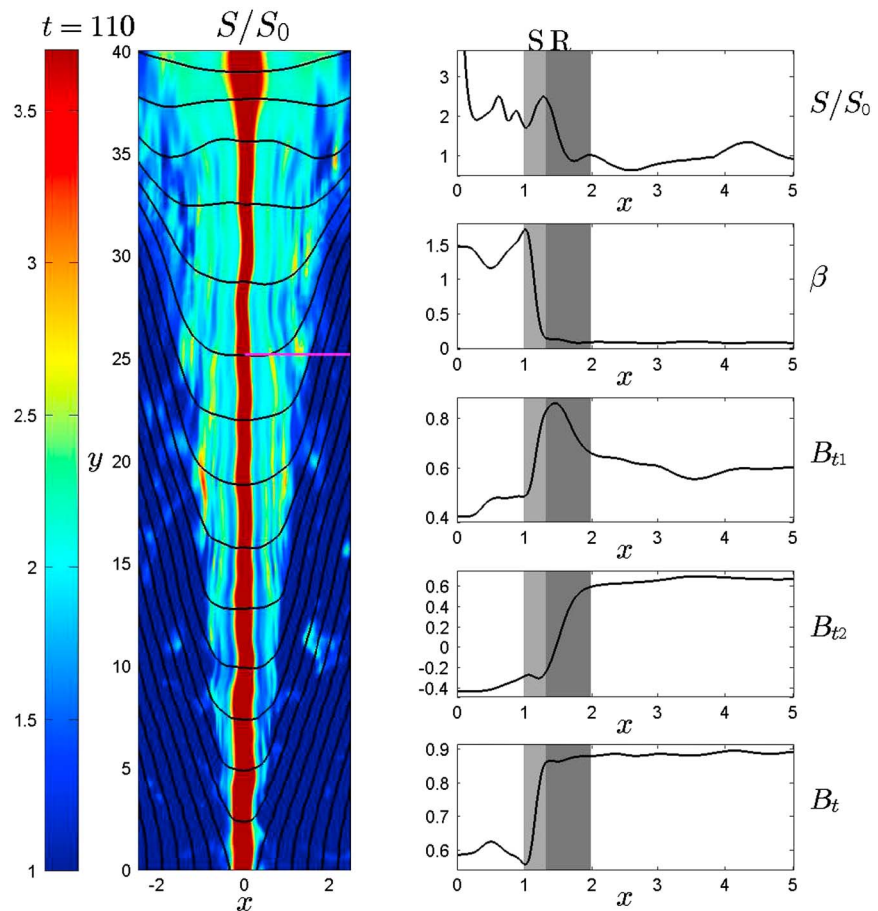
Figure 8. (left) The normalized entropy at $t = 110$. Black lines are the magnetic field lines. (right) The five panels show the profiles of the normalized entropy, plasma beta, two components of the tangential magnetic field B_{t1} and B_{t2}, and the total tangential magnetic field, which are taken from the magenta line in Figure 8 (left).

magnetic field strongly deceases. This remnant magnetic field, however, is still larger than the y component of the magnetic field B_y in the inflow region. The larger B_y field implies a smaller increase of the thermal pressure in the outflow region, and for this reason, a reduction in the entropy increases. Therefore, Case C demonstrates that the presence of a guide field reduces the entropy increase.

4.3. Magnetic Reconnection With Shear Flow

Large shear flow always exists close to the magnetopause, due to the solar wind velocity. This sheared flow general has components along the y and z directions, and here we consider shear along the z (invariant in the two-dimensional configuration) direction. Flow shear along the y direction has an effect similar to density asymmetry in that it generates a configuration similar to density asymmetry with a nonzero B_y in the outflow region [*La Belle-Hamer et al.*, 1995]. For flow shear along the z direction, the frozen-in condition implies a drag of reconnected magnetic field lines into opposite directions on the two sides of the outflow region, which generates a B_z component. This B_z component contributes an additional magnetic pressure to the total pressure in the steady outflow region. This mechanism is demonstrated in Case D, where the initial configuration is the same as in Case A, except for the perpendicular flow shear. In Case D, the total perpendicular velocity jump is equal to the Alfvén speed. Figure 8 (left) shows the normalized entropy S/S_0 at $t = 110$, where S_0 is the inflow entropy. The figure shows that the outflow entropy is about twice the inflow entropy, which is lower than in Case A. Similar to the guide field case, the presence of the shear flow replaces the switch-off shock by an intermediate shock and a slow shock [*Sun et al.*, 2005]. The five panels in Figure 8 (right) show the profiles of the normalized entropy, plasma beta, two components of the tangential magnetic field B_{t1} and B_{t2}, and the total tangential magnetic field, which are taken from the magenta line in Figure 7 (left). Due to the symmetry, we only show the $x \geq 0$ part of the cut. For a better representation of the intermediate shock, we rotated the frame by an angle $\theta = \pi/4$. The entropy increases through the

intermediate shock layer and the slow shock layer. Again, the magnetic pressure in the outflow region reduces the thermal pressure and the entropy increase.

5. Summary and Discussion

The plasma entropy measure p/ρ^γ is a useful physical quantity to identify adiabatic and nonadiabatic processes in a physical system, and satellite observations demonstrate that the access of solar wind plasma to the Earth's magnetosphere involves strong nonadiabatic heating. Magnetic reconnection is often suggested as the dominant process for this transport of plasma into the magnetosphere. In this study, we focus mainly on Petschek-type magnetic reconnection, and we demonstrate that entropy can strongly increase only when the plasma $\beta \ll 1$ by means of theoretical analysis and numerical simulation using one-dimensional and two-dimensional configurations. Key arguments for this β limitation are (1) that the compression rate is usually around unity ($\rho_d/\rho_u = \mathcal{O}(1)$) and (2) that the thermal pressure is limited by the total pressure in an approximately pressure balanced system. A large entropy increase in such a total pressure balanced system requires a very small thermal pressure (compared to magnetic pressure) in the inflow region. It can be expected that the beta limitation for the entropy increase is applicable also to kinetic models of reconnection as long as such models satisfy approximate total pressure balance and plasma compression of order unity.

The more specific quantitative estimates of entropy changes are mostly based on applications of steady state reconnection. Frequently, reconnection is considered to be a time-dependent process (such as the formation of magnetic flux transfer events (FTEs) [*Russell and Elphic*, 1978, 1979] or plasmoids in the terrestrial magnetosphere [*Hones et al.*, 1984; *Moldwin and Hughes*, 1992]). It is trivial that a steady state assumption is always violated on sufficiently large spatial or temporal scales. A steady state is defined by the condition that system changes are slow (time scale τ_r) compared to typical wave travel times τ_L across the system. For a reconnection geometry, this implies $\tau_L << \tau_r$ with $\tau_L = d/V$, (d is the width of the outflow region and V is the speed of group velocity of typical wave), and $\tau_r = r(dr/dt)^{-1}$ is characterized by the change of the reconnection rate r. For instance, the scale size of typical FTEs [*Kawano and Russell*, 1996] or typical plasmoids in the magnetotail [*Ieda et al.*, 1998; *Imber et al.*, 2011] requires several minutes of sustained fast reconnection. The Alfvén speed in these region is typically 100 to several 100 km s^{-1}, such that typical wave travel times are of the order of 10 s, i.e., much shorter than the required duration of fast reconnection. It is also noted that the asymmetric current layers for magnetopause reconnection and for large-scale solar wind reconnection events [*Eriksson et al.*, 2009] appear reasonably consistent with basic predictions by MHD reconnection.

In two-dimensional MHD magnetic reconnection, the entropy increase occurs mostly through the shock layers. Such shocks do not exist or are modified in the presence of kinetic physics [*Lin and Lee*, 1993; *Lin*, 2001; *Hesse et al.*, 2008; *Ma and Otto*, 2013; *Zenitani et al.*, 2013], which may involve additional entropy sources/sinks. However, kinetic models are still governed by the fundamental conservation laws (i.e., mass, energy, and momentum conservation). Therefore, the asymptotic behavior on sufficiently large scales of the transition from the inflow to the outflow region should be somewhat consistent with the MHD shock prediction provided that the plasma remains sufficiently isotropic. This is an ultimately unresolved problem worthy of a more detailed large-scale kinetic study.

Other entropy sources include the small reconnection diffusion region which can heat plasma locally. However, it has no volume filling effect because of its microscopic (ion or electron inertia scale) size. A fast shock may exist in the transition region between steady outflow region and nonsteady bulge region, when the inflow plasma beta is low. However, the Mach number is too small (marginally above 1), such that the fast shock is not expected to be a major entropy source.

For more realistic configuration, density asymmetry leads to $B_y \neq 0$ in the outflow region which reduces the entropy increase. The presence of a guide field and a perpendicular shear flow also reduce the entropy increase in the outflow region. This reduction of nonadiabatic heating is caused the replacement of the switch-off shock in the steady outflow region by a rotational discontinuity (or intermediate shock) and a slow shock, which does not switch off the tangential component of the magnetic field for both configurations. Therefore, any asymmetry, guide field, or shear flow increases the magnetic field magnitude in the outflow region and reduces the thermal pressure increase from the inflow to the outflow regions, which results in a lower entropy increase than in the symmetric (Petschek) situation.

The presented results demonstrate that magnetic reconnection can indeed generate a strong nonadiabatic heating. However, the condition for this is a sufficiently small plasma $\beta \ll 1$. Typical magnetosheath conditions imply a plasma beta of order 0.1 to 1. This is insufficient to explain the observed entropy increase of at least 1 to 2 orders of magnitude between the magnetosheath and the magnetosphere. It is also noted that reconnection causes plasma compression where the original magnetosheath densities are already too high in comparison with plasma sheet. A subsequent adiabatic expansion would lower the temperature of the plasma far below values observed in the magnetosphere. Therefore, it is concluded that additional physics is required to explain density and temperature of the plasma sheet. Such physics can include the following: (1) plasma conditions that are not typical magnetosheath. For instance, density and plasma beta are typically significantly lower in the plasma depletion layer just outside of the magnetopause, (2) plasma conditions that are modified by additional processes such of Kelvin-Helmholtz instability, and (3) other processes that contribute to the plasma entry, such as diffusion or other microphysical processes [*Johnson and Wing*, 2009].

There are two additional highly important applications for low-beta reconnection. In the magnetotail lobes (similar in other magnetospheres such as the giant planets), the plasma beta is extraordinarily low. Here reconnection of lobe magnetic field can be expected to increase the entropy very significantly by orders of magnitude. Observations indicate that bursty earthward directed flows are likely entropy-depleted flux tubes, which are generated by lobe reconnection because of the low lobe plasma beta [*Angelopoulos et al.*, 1992; *Birn et al.*, 2011]. However, observations indicate that only few of these flows have a sufficiently low flux tube entropy to reach geosynchronous distances where particle injection is observed during substorms [*Sergeev et al.*, 2012; *Kim et al.*, 2012; *Dubyagin et al.*, 2011]. A significant nonadiabatic heating in the outflow region is a critical element to better understand the penetration depth of such reconnection flows [*Lyons et al.*, 2009]. The second application is reconnection in the solar corona where again the plasma beta is very low, and magnetic reconnection can potentially increase the plasma entropy by orders of magnitude.

References

Angelopoulos, V., W. Baumjohann, C. F. Kennel, F. V. Coronti, M. G. Kivelson, R. Pellat, R. J. Walker, H. Luehr, and G. Paschmann (1992), Bursty bulk flows in the inner central plasma sheet, *J. Geophys. Res.*, *97*, 4027–4039, doi:10.1029/91JA02701.

Balasis, G., I. A. Daglis, C. Papadimitriou, M. Kalimeri, A. Anastasiadis, and K. Eftaxias (2009), Investigating dynamical complexity in the magnetosphere using various entropy measures, *J. Geophys. Res.*, *114*, A00D06, doi:10.1029/2008JA014035.

Biernat, H. K., V. S. Semenov, O. A. Drobysh, and M. F. Heyn (1998), Magnetic reconnection: Observations on October 29, 1979, and model results, *J. Geophys. Res.*, *103*(A6), 11,919–11,927, doi:10.1029/98JA00587.

Birn, J., M. Hesse, and K. Schindler (2006), Entropy conservation in simulations of magnetic reconnection, *Phys. Plasmas*, *13*(9), 092,117, doi:10.1063/1.2349440.

Birn, J., M. Hesse, K. Schindler, and S. Zaharia (2009), Role of entropy in magnetotail dynamics, *J. Geophys. Res.*, *114*, A00D03, doi:10.1029/2008JA014015.

Birn, J., R. Nakamura, E. V. Panov, and M. Hesse (2011), Bursty bulk flows and dipolarization in MHD simulations of magnetotail reconnection, *J. Geophys. Res.*, *116*, A01210, doi:10.1029/2010JA016083.

Borovsky, J. E., and T. E. Cayton (2011), Entropy mapping of the outer electron radiation belt between the magnetotail and geosynchronous orbit, *J. Geophys. Res.*, *116*, A06216, doi:10.1029/2011JA016470.

Dubyagin, S., V. Sergeev, S. Apatenkov, V. Angelopoulos, A. Runov, R. Nakamura, W. Baumjohann, J. McFadden, and D. Larson (2011), Can flow bursts penetrate into the inner magnetosphere?, *Geophys. Res. Lett.*, *38*, L08102, doi:10.1029/2011GL047016.

Dungey, J. W. (1961), Interplanetary magnetic field and the auroral zones, *Phys. Rev. Lett.*, *6*, 47–48, doi:10.1103/PhysRevLett.6.47.

Eriksson, S., et al. (2009), Asymmetric shear flow effects on magnetic field configuration within oppositely directed solar wind reconnection exhausts, *J. Geophys. Res.*, *114*, A07103, doi:10.1029/2008JA013990.

Fujimoto, M., T. Terasawa, and T. Mukai (1997), The cold-dense plasma sheet: A Geotail perspective, *Space Sci. Rev.*, *80*, 325–339, doi:10.1023/A:1004934306623.

Harris, E. (1962), On a plasma sheath separating regions of oppositely directed magnetic field, *Nuovo Cimento*, *23*(1), 115–121, doi:10.1007/BF02733547.

Hesse, M., J. Birn, and M. Kuznetsova (2001), Collisionless magnetic reconnection: Electron processes and transport modeling, *J. Geophys. Res.*, *106*(A3), 3721–3735, doi:10.1029/1999JA001002.

Hesse, M., S. Zenitani, and A. Klimas (2008), The structure of the electron outflow jet in collisionless magnetic reconnection, *Phys. Plasmas*, *15*(11), 112,102, doi:10.1063/1.3006341.

Hones, E. W., J. Birn, D. N. Baker, S. J. Bame, W. C. Feldman, D. J. McComas, R. D. Zwickl, J. A. Slavin, E. J. Smith, and B. T. Tsurutani (1984), Detailed examination of a plasmoid in the distant magnetotail with ISEE 3, *Geophys. Res. Lett.*, *11*(10), 1046–1049, doi:10.1029/GL011i010p01046.

Ieda, A., S. Machida, T. Mukai, Y. Saito, T. Yamamoto, A. Nishida, T. Terasawa, and S. Kokubun (1998), Statistical analysis of the plasmoid evolution with Geotail observations, *J. Geophys. Res.*, *103*(A3), 4453–4465, doi:10.1029/97JA03240.

Imber, S. M., J. A. Slavin, H. U. Auster, and V. Angelopoulos (2011), A THEMIS survey of flux ropes and traveling compression regions: Location of the near-Earth reconnection site during solar minimum, *J. Geophys. Res.*, *116*, A02201, doi:10.1029/2010JA016026.

Johnson, J. R., and S. Wing (2009), Northward interplanetary magnetic field plasma sheet entropies, *J. Geophys. Res.*, *114*, A00D08, doi:10.1029/2008JA014017.

Kaufmann, R. L., and W. R. Paterson (2009), Boltzmann *h* function and entropy in the plasma sheet, *J. Geophys. Res.*, *114*, A00D04, doi:10.1029/2008JA014030.

Kawano, H., and C. T. Russell (1996), Survey of flux transfer events observed with the ISEE 1 spacecraft: Rotational polarity and the source region, *J. Geophys. Res.*, *101*(A12), 27,299–27,308, doi:10.1029/96JA02703.

Kessel, R. L., S.-H. Chen, J. L. Green, S. F. Fung, S. A. Boardsen, L. C. Tan, T. E. Eastman, J. D. Craven, and L. A. Frank (1996), Evidence of high-latitude reconnecting during northward IMF: Hawkeye observations, *Geophys. Res. Lett.*, *23*, 583–586, doi:10.1029/95GL03083.

Kim, H.-S., D.-Y. Lee, S. Ohtani, M.-Y. Park, and B.-H. Ahn (2012), On near-tail bubble penetration into geosynchronous altitude, *J. Geophys. Res.*, *117*, A07205, doi:10.1029/2012JA017749.

La Belle-Hamer, A. L., A. Otto, and L. C. Lee (1995), Magnetic reconnection in the presence of sheared flow and density asymmetry: Applications to the Earth's magnetopause, *J. Geophys. Res.*, *100*, 11,875–11,889, doi:10.1029/94JA00969.

Lin, Y. (2001), Global hybrid simulation of the dayside reconnection layer and associated field-aligned currents, *J. Geophys. Res.*, *106*, 25,451–25,466, doi:10.1029/2000JA000184.

Lin, Y., and L. C. Lee (1993), Structure of reconnection layers in the magnetosphere, *Space Sci. Rev.*, *65*, 59–179, doi:10.1007/BF00749762.

Lin, Y., and L. C. Lee (1999), Reconnection layers in two-dimensional magnetohydrodynamics and comparison with the one-dimensional Riemann problem, *Phys. Plasmas*, *6*, 3131–3146, doi:10.1063/1.873553.

Lyons, L. R., C.-P. Wang, M. Gkioulidou, and S. Zou (2009), Connections between plasma sheet transport, Region 2 currents, and entropy changes associated with convection, steady magnetospheric convection periods, and substorms, *J. Geophys. Res.*, *114*, A00D01, doi:10.1029/2008JA013743.

Ma, X., and A. Otto (2013), Mechanisms of field-aligned current formation in magnetic reconnection, *J. Geophys. Res. Space Physics*, *118*, 4906–4914, doi:10.1002/jgra.50457.

Ma, Z. W., and A. Bhattacharjee (2001), Hall magnetohydrodynamic reconnection: The Geospace Environment Modeling challenge, *J. Geophys. Res.*, *106*, 3773–3782, doi:10.1029/1999JA001004.

Moldwin, M. B., and W. J. Hughes (1992), On the formation and evolution of plasmoids: A survey of ISEE 3 Geotail data, *J. Geophys. Res.*, *97*(A12), 19,259–19,282, doi:10.1029/92JA01598.

Otto, A. (1990), 3D resistive MHD computations of magnetospheric physics, *Comput. Phys. Commun.*, *59*, 185–195, doi:10.1016/0010-4655(90)90168-Z.

Otto, A. (2012), *Advanced Plasma Physics Lecture Notes*. [Available at http://how.gi.alaska.edu/ao/adv_plasma/.]

Otto, A., J. Büchner, and B. Nikutowski (2007), Force-free magnetic field extrapolation for MHD boundary conditions in simulations of the solar atmosphere, *A & A*, *468*, 313–321, doi:10.1051/0004-6361:20054495.

Parker, E. N. (1957), Sweet's mechanism for merging magnetic fields in conducting fluids, *J. Geophys. Res.*, *62*, 509–520, doi:10.1029/JZ062i004p00509.

Petschek, H. E. (1964), Magnetic field annihilation, in *The Physics of Solar Flares, Proceedings of the AAS-NASA Symposium held 28–30 October, 1963 at the Goddard Space Flight Center, Greenbelt, MD*, vol. 50, edited by W. N. Hess, 425 pp., *NASA Spec. Publ.*, Washington, D. C.

Pritchett, P. L. (2001), Geospace environment modeling magnetic reconnection challenge: Simulations with a full particle electromagnetic code, *J. Geophys. Res.*, *106*(A3), 3783–3798, doi:10.1029/1999JA001006.

Russell, C. T., and R. C. Elphic (1978), Initial ISEE magnetometer results: Magnetopause observations, *Space Sci. Rev.*, *22*, 681–715, doi:10.1007/BF00212619.

Russell, C. T., and R. C. Elphic (1979), ISEE observations of flux transfer events at the dayside magnetopause, *Geophys. Res. Lett.*, *6*, 33–36, doi:10.1029/GL006i001p00033.

Scholer, M., and R. A. Treumann (1997), The low-latitude boundary layer at the flanks of the magnetopause, *Space Sci. Rev.*, *80*, 341–367, doi:10.1023/A:1004986323461.

Sergeev, V. A., I. A. Chernyaev, S. V. Dubyagin, Y. Miyashita, V. Angelopoulos, P. D. Boakes, R. Nakamura, and M. G. Henderson (2012), Energetic particle injections to geostationary orbit: Relationship to flow bursts and magnetospheric state, *J. Geophys. Res.*, *117*, A10207, doi:10.1029/2012JA017773.

Shay, M. A., J. F. Drake, B. N. Rogers, and R. E. Denton (2001), Alfvénic collisionless magnetic reconnection and the Hall term, *J. Geophys. Res.*, *106*(A3), 3759–3772, doi:10.1029/1999JA001007.

Sun, X., Y. Lin, and X. Wang (2005), Structure of reconnection layer with a shear flow perpendicular to the antiparallel magnetic field component, *Phys. Plasmas*, *12*(1), 012305, doi:10.1063/1.1826096.

Sweet, P. A. (1958), The neutral point theory of solar flares, in *Electromagnetic Phenomena in Cosmical Physics, Proceedings From IAU Symposium No. 6*, edited by B. Lehnert, 123 pp., Cambridge Univ. Press, Cambridge, U. K.

Walthour, D. W., B. U. O. Sonnerup, and C. T. Russell (1995), Observation of a slow-mode shock in the dayside magnetopause reconnection layer, *Adv. Space Res.*, *15*, 501–506, doi:10.1016/0273-1177(94)00135-N.

Wang, C.-P., L. R. Lyons, T. Nagai, J. M. Weygand, and R. W. McEntire (2007), Sources, transport, and distributions of plasma sheet ions and electrons and dependences on interplanetary parameters under northward interplanetary magnetic field, *J. Geophys. Res.*, *112*, A10224, doi:10.1029/2007JA012522.

Wing, S., and J. R. Johnson (2009), Substorm entropies, *J. Geophys. Res.*, *114*(A9), A00D07, doi:10.1029/2008JA013989.

Wu, B. H., and L. C. Lee (2000), Hall effects on the Walén relation in rotational discontinuities and Alfvén waves, *J. Geophys. Res.*, *105*, 18,377–18,390, doi:10.1029/2000JA900043.

Yang, H. A., S. P. Jin, and G. C. Zhou (2006), Density depletion and Hall effect in magnetic reconnection, *J. Geophys. Res.*, *111*, A11223, doi:10.1029/2005JA011536.

Yong, S., and L. C. Lee (1990), Structure of the reconnection layer at the dayside magnetopause, *Planet. Space Sci.*, *38*, 437–458, doi:10.1016/0032-0633(90)90109-4.

Zenitani, S., and T. Miyoshi (2011), Magnetohydrodynamic structure of a plasmoid in fast reconnection in low-beta plasmas, *Phys. Plasmas*, *18*(2), 022105, doi:10.1063/1.3554655.

Zenitani, S., I. Shinohara, T. Nagai, and T. Wada (2013), Kinetic aspects of the ion current layer in a reconnection outflow exhaust, *Phys. Plasmas*, *20*(9), 092120, doi:10.1063/1.4821963.